A BD FACS Aria (BD Immunocytometry Systems, San Jose, CA, USA) was used for all multi-color FACS analysis and cell sorting. Data were analyzed using FlowJo software (Treestar, San Carlos, CA, USA).

Quantification of HTLV-I proviral load by real-time quantitative polymerase chain reaction (PCR). The HTLV-I proviral load in PBMC was quantified by real-time quantitative polymerase chain reaction (PCR; TaqMan method) using the ABI Prism 7000 sequence detection system (Applied Biosystems, Foster

City, CA, USA) as previously described.[13] Briefly, a total of 50 ng of genomic DNA was extracted from human PBMC using a QIAamp DNA blood Micro kit (Qiagen, Hilden, Germany). Triplicate samples of the DNA were amplified. Each PCR mixture containing a HTLV-I pX region-specific primer pair at 0.1 μM (forward primer 5′-CGGATACCCAGTCTACGTGTT-3′ and reverse primer 5′-CAGTAGGGCGTGACGATGTA-3′), FAM-labeled probe at 0.1 μM (5′- CTGTGTACAAGGC-GACTGGTGCC-3′) and 1× TaqMan Universal PCR master mix
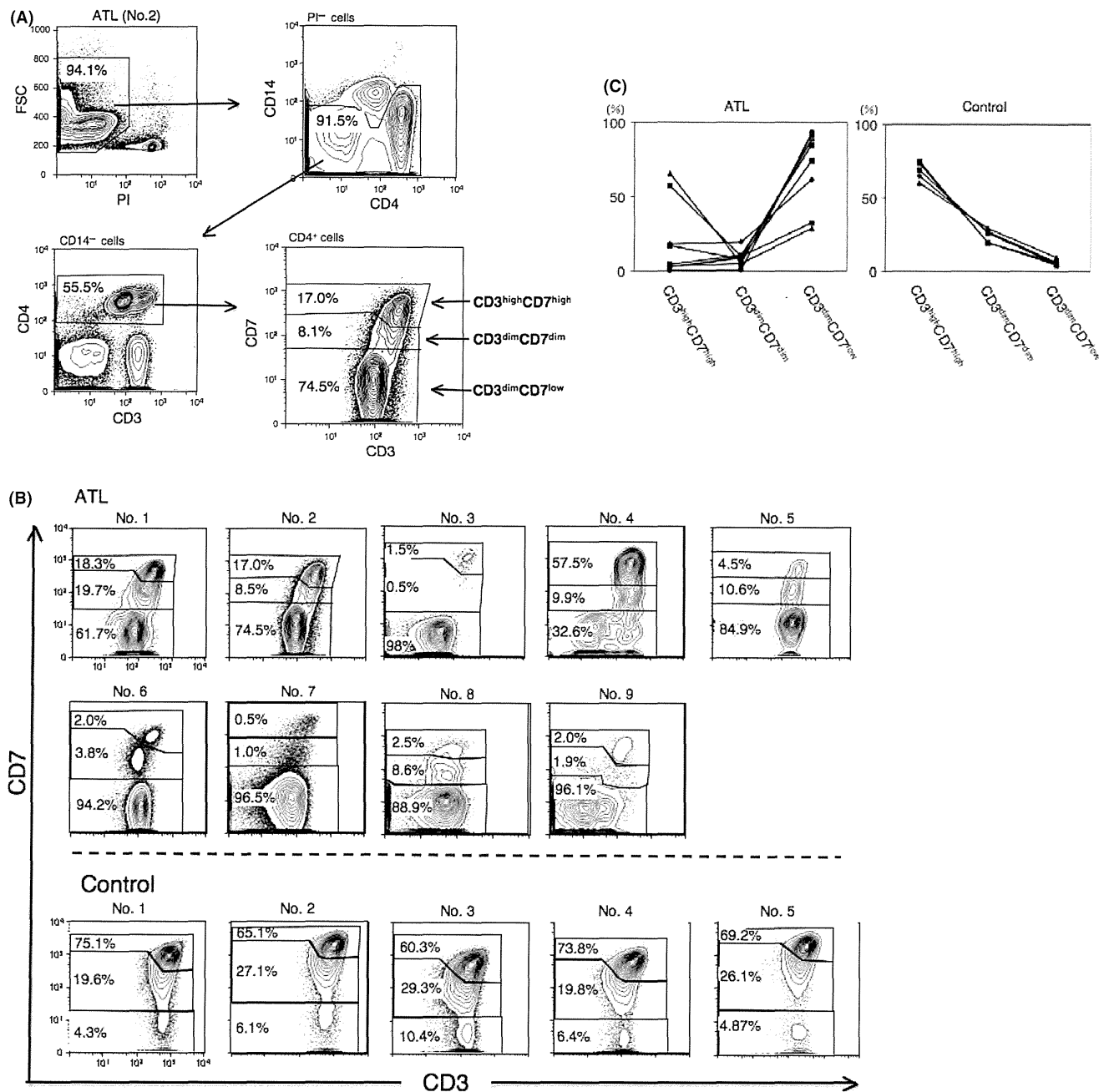

Fig. 1. CD3 vs CD7 plots from FACS analysis of patients with acute-type adult T-cell leukemia (ATL) and normal controls. (A) Representative flow cytometric analysis of a patient with acute-type ATL (patient no. 2). The CD3 vs CD7 plot in CD4+ cells was constructed according to the gating procedure shown in this figure. In the plot, we designated three subpopulations: CD3^high^CD7^high^, CD3^dim^CD7^dim^ and CD3^dim^CD7^low^. (B) Flow cytometric profile of the CD3 vs CD7 plot in patients with acute-type ATL and normal controls. (C) Percentages of CD3^high^CD7^high^, CD3^dim^CD7^dim^ and CD3^dim^CD7^low^ subpopulations in CD4+ T cells in patients with acute-type ATL and normal controls. Each line represents an individual sample. ATL group, n = 9; control group, n = 5; FSC, forward scatter; PI, Propidium iodide.

Table 1. Clinical profile of nine acute-type ATL patients in the present study

No.	Age	Sex	WBC (/μL)	Lymph (%)	ATL cellst (%)	Organ involvement
1	60	M	5200	15.0	11.0	Skin
2	69	F	1600	43.5	9.0	Liver, LN, pleural effusion
3	61	M	18 620	24.7	43.7	Liver, uvea
4	59	F	6420	8.5	0.0	Liver, LN, skin
5	70	F	290	56.0	2.0	Liver, spleen, LN
6	60	F	4570	19.0	73.0	Skin
7	53	F	12 210	11.0	52.0	LN
8	74	F	6480	16.5	25.5	Liver, spleen, LN
9	63	F	34 810	21.5	33.5	Liver, spleen, LN, lung

†Proportion of ATL cells in the peripheral blood WBC evaluated by morphological examination. ATL, adult T-cell leukemia; LN, lymph nodes; Lymph, lymphocytes; WBC, white blood cells (normal range, 3500–9100/μL).

(Applied Biosystems) were subjected to 50 cycles of denaturation (95°C, 15 s) and annealing to extension (60°C, 1 min), following an initial Taq polymerase activation step (95°C, 10 min). The RNase P control reagent (Applied Biosystems) was used as an internal control for calculation of the input cell number (using VIC reporter dye). DNA extracted from TL-Om1 and normal human PBMC were used as positive and negative controls, respectively. The HTLV-I proviral load (%) was calculated as the copy number of the pX region per input cell number. To correct the deviation of acquired data in each experiment, data from TL-Om1 (positive control) were adjusted to 100% and the sample data was corrected by proportional calculation accordingly.

Inverse long PCR. For clonality analysis, inverse long PCR was performed. First, 1 μg of genomic DNA extracted from the FACS-sorted cells was digested with *Eco*RI, *Hin*dIII and *Pst*I at 37°C overnight. Purification of DNA fragments was performed using a QIAEX2 gel extraction kit (Qiagen). The purified DNA was self-ligated with T4 DNA ligase (Takara Bio, Otsu, Japan) at 16°C overnight. The circular DNA obtained from the *Eco*RI digestion fragment was then digested with *Mlu*I, which cuts the pX region of the HTLV-I genome and prevents amplification with the viral genome. Inverse long PCR was performed using Takara LA *Taq* polymerase (Takara Bio). The primer pairs for the *Eco*RI-treated template were: forward primer 5′-TGCCT-GACCCTGCTTGCTCAACTCTACGTCTTTG-3′ and reverse primer 5′-AGTCTGGGCCCTGACCTTTTCAGACTTCTGTT-TC-3′. For the *Hin*dIII-treated group, forward primer 5′-TAG-

CAGGAGTCTATAAAAGCGTGGAGACAG-3′ and reverse primer 5′-TGGGCAGGATTGCAGGGTTTAGAGTGG-3′ were used. For the *Pst*I-treated group, forward primer 5′-CAG-CCCATTCTATAGCACTCTCCAGGAGAG-3′ and reverse primer 5′-CAGTCTCCAAACACGTAGACTGGGTATCCG-3 were used. Each 50-μL reaction mixture contained 0.4 mM of each dNTP, 25 mM $MgCl_2$, 10× LA PCR buffer II containing 20 mM Tris–HCl and 100 mM KCl, 0.5 mM primer, 2.5 U LA *Taq* polymerase and 50 ng of the processed genomic DNA. The reaction mixture of the *Eco*RI- or *Pst*I-treated group was subjected to 35 cycles of denaturation (94°C, 30 s) and annealing to extension (68°C, 8 min). For the *Hin*dIII group, the PCR conditions were denaturation (98°C, 30 s), annealing to extension (64°C, 10 min) for 5 cycles, followed by 30 cycles of denaturation (94°C, 30 s), annealing (64°C, 3 min) and extension (72°C, 15 min). Following PCR, the products were subjected to electrophoresis in 0.8% agarose gels. In the $CD3^{dim}CD7^{low}$ subpopulation from which a sufficient amount of DNA was extracted, PCR were performed in duplicate.

Cytospin and May–Giemsa staining. Cells enriched by cell sorting were washed twice with PBS. Aliquots of 100 μL of the cell suspension were mixed with 20 μL of 10% bovine serum albumin. The mixtures were centrifuged at 20*g* for 5 min onto glass slides. The fixed cells were air-dried and then subjected to May–Giemsa staining.

Statistical analyses. Data are expressed as the means ± standard deviation (SD). One-way analysis of variance (ANOVA) was used for statistical analyses, and $P < 0.05$ was taken to indicate statistical significance.

Results

Multi-color FACS, including CD3 *vs* CD7 plots, in patients with acute-type ATL. We constructed a gating procedure for flow cytometric analysis of acute-type ATL cells using a combination of CD3 and CD7. Figure 1A shows the representative flow cytometric data of an ATL sample (from patient no. 2 in Table 1). Dead cells (PI positive) were initially excluded on the forward scatter (FSC) *vs* PI plot. Next, monocytes ($CD4^{dim}$ $CD14^+$) were excluded on the CD4 *vs* CD14 plot. After $CD4^+$ T lymphocytes were gated on the CD3 *vs* CD4 plot, a CD3 *vs* CD7 plot was constructed. Based on the cell density and fluorescence intensity of CD3 and CD7, we designated three subpopulations on this plot: $CD3^{high}CD7^{high}$, $CD3^{dim}CD7^{dim}$ and $CD3^{dim}CD7^{low}$ (Fig. 1A). Using the same gating procedure, we analyzed nine patients with acute-type ATL and five normal controls (Fig. 1B). The patient characteristics analyzed in the present study are shown in Table 1. In normal controls, the expression pattern of CD3 *vs* CD7 was similar. The highest cell density was observed in the $CD3^{high}CD7^{high}$ subpopulation, and the $CD3^{dim}CD7^{dim}$ subpopulation was observed adjacent to it. The $CD3^{dim}CD7^{low}$
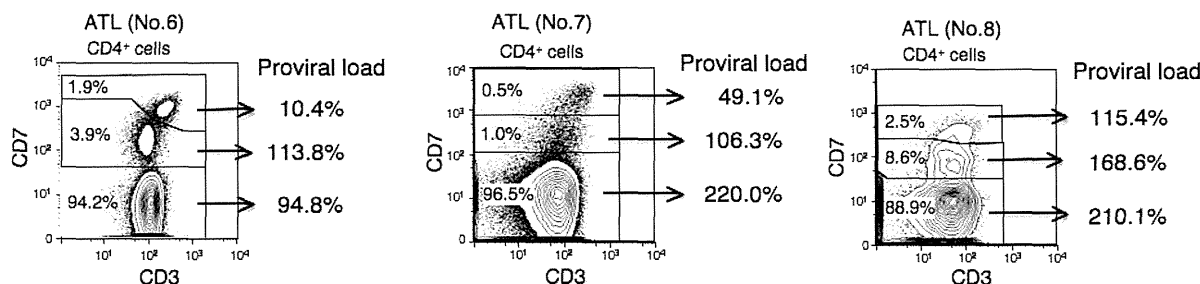

Fig. 2. Quantification of the human T-cell leukemia virus type 1 (HTLV-I) proviral load in $CD3^{high}CD7^{high}$, $CD3^{dim}CD7^{dim}$ and $CD3^{dim}CD7^{low}$ subpopulations. Genomic DNA was extracted from the FACS-sorted cells of each subpopulation and subjected to real-time quantitative PCR. Representative data of three cases (patients no. 6, 7 and 8) are shown.

subpopulation was a minor but distinct subpopulation. In contrast, the highest cell density was observed in the $CD3^{dim}CD7^{low}$ subpopulation in all acute-type ATL samples except for patient no. 4, from whom the sample was obtained under conditions of well-controlled ATL during chemotherapy. These subpopulations were distinct but the expression pattern of the CD3 vs CD7 plot, such as the degree of downregulation of CD3 and CD7, was variable among patients. The proportion of the $CD3^{dim}CD7^{low}$ subpopulation was significantly higher in acute-type ATL $CD4^+$ lymphocytes than in normal controls (Fig. 1C).

Analysis of the HTLV-I proviral load in $CD3^{high}CD7^{high}$, $CD3^{dim}CD7^{dim}$ and $CD3^{dim}CD7^{low}$ subpopulations. We next estimated the HTLV-I proviral load by quantitative real-time PCR in each FACS-sorted subpopulation. Representative results from three patients with acute-type ATL (patients no. 6, 7 and 8) are shown in Figure 2. In all patient samples, HTLV-I proviral integration, analyzed by real-time PCR, was detected in all subpopulations. However, the proviral load (%) was significantly

higher in $CD3^{dim}CD7^{dim}$ and $CD3^{dim}CD7^{low}$ subpopulations compared with the $CD3^{high}CD7^{high}$ subpopulation. The proviral load of the $CD3^{dim}CD7^{low}$ subpopulation in patients no. 7 and 8 was nearly 200%, indicating integration of two copies of the HTLV-I viral genome and that almost all of the cells were infected with HTLV-I. Similarly, in patient no. 6, the majority of the $CD3^{dim}CD7^{low}$ subpopulation was infected with HTLV-I. A substantial proportion of the $CD3^{dim}CD7^{dim}$ subpopulation was infected with HTLV-I in patients no. 7 and 8, and nearly all the cells in the same subpopulation in patient no. 6 were infected with HTLV-I.

Differences in the immunophenotype of $CD3^{high}CD7^{high}$, $CD3^{dim}CD7^{dim}$ and $CD3^{dim}CD7^{low}$ subpopulations in patients with acute-type ATL. To further characterize these three subpopulations, we next examined CCR4 and CD25 expression in each subpopulation. Representative results of a normal control and a patient with acute-type ATL are shown in Figure 3A. The mean fluorescence intensities (MFI) of CD25 and CCR4 of each sub-
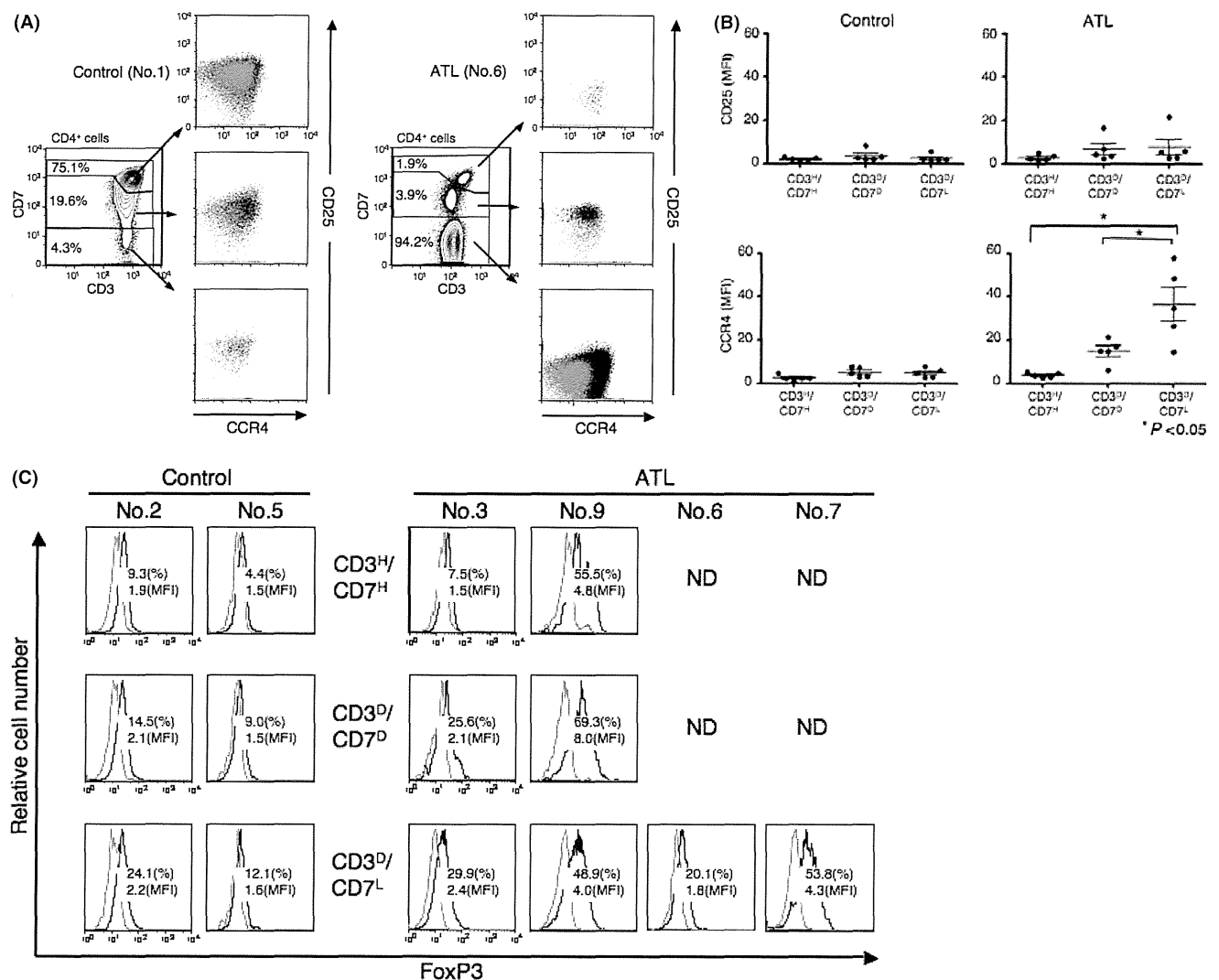

Fig. 3. Immunophenotypic analysis in $CD3^{high}CD7^{high}$, $CD3^{dim}CD7^{dim}$ and $CD3^{dim}CD7^{low}$ subpopulations. (A) Expression of CCR4 and CD25 in each subpopulation. Representative FACS data of a normal control (no. 1) and a patient with adult T-cell leukemia (ATL) (no. 6) are shown Gray dots, isotype antibody-stained cells; black dots, specific antibody-stained cells. (B) Mean fluorescence intensity (MFI) of CD25 and CCR4 in each subpopulation from all normal controls and patients with ATL. The MFI is shown in arbitrary units defined as follows: MFI of specific antibody/MFI of isotype antibody. Each dot represents a sample *P < 005 by ANOVA. (C) Expression of FoxP3 in each subpopulation. ND, analysis could not be performed in the $CD3^{high}CD7^{high}$ and $CD3^{dim}CD7^{dim}$ subpopulations in patients no. 6 and 7 due to an insufficient number of cells.

population in all patients with ATL and normal controls are shown in Figure 3B. Both CCR4 and CD25 expression levels were very low and maintained at similar levels throughout all subpopulations in normal control cells and in the CD3^{high}CD7^{high} subpopulation of patients with ATL. In contrast, CCR4 expression was significantly upregulated in the CD3^{dim}CD7^{dim} and CD3^{dim}CD7^{low} subpopulations of patients with ATL compared with the CD3^{high}CD7^{high} subpopulation. The expression of CD25 was also upregulated in these subpopulations but this difference was not significant ($P = 0.36$). The expression of Forkhead box P3 (FoxP3), a master regulator in the development and function of regulatory T (Treg) cells,[14] was also analyzed in some patients. As shown in Figure 3C, FoxP3 expression in the CD3^{dim}CD7^{low} subpopulations was variably upregulated among patients. In addition, in patient no. 9, FoxP3 was upregulated in the CD3^{high}CD7^{high} and CD3^{dim}CD7^{dim} subpopulations.

Analysis of clonality in the CD3^{high}CD7^{high}, CD3^{dim}CD7^{dim} and CD3^{dim}CD7^{low} subpopulations by inverse long PCR. To further analyze the enrichment of ATL cells in the CD3^{dim}CD7^{low} subpopulation, we estimated clonality in each FACS-sorted subpopulation by inverse long PCR in four patients with acute-type ATL (Fig. 4). An intense band, suggesting a major clone, was detected in the CD3^{dim}CD7^{low} subpopulations in all patients. In the same subpopulation, multiple bands with weak intensity were also observed. As the levels of DNA extracted from the CD3^{dim}CD7^{low} subpopulation were sufficient, we performed duplicate PCR in three patient samples (Fig. 4B–D). Detection of the major bands was consistent, but the presence of the minor bands was variable. In the CD3^{dim}CD7^{dim} subpopulations, bands of the same size as those of the CD3^{dim}CD7^{low} subpopulations were observed, indicating that a distinct population in the CD3^{dim}CD7^{dim} subpopulations belonged to identical clones.

Clonality in the CD3^{high}CD7^{high}, CD3^{dim}CD7^{dim} and CD3^{dim}CD7^{low} subpopulations by flow cytometry-based TCR-Vβ repertoire analysis. To further confirm clonality and to evaluate the degree of enrichment in each subpopulation, we performed TCR-Vβ repertoire analysis by flow cytometry[15] in three ATL cases. The representative results are shown in Figure 5. In patient no. 3, over 95% of the CD3^{dim}CD7^{low} subpopulation used specific TCR-Vβ (Vβ9) and their proportion was quite low in the CD3^{high}CD7^{high} and CD3^{dim}CD7^{dim} subpopulations. In addition, in the two other cases, over 90% of cells in the CD3^{dim}CD7^{low} subpopulation used the same TCR-Vβ (data not shown). These results indicate that ATL cells are highly purified in the CD3^{dim}CD7^{low} subpopulation.

Differences in morphology of the CD3^{high}CD7^{high}, CD3^{dim}CD7^{dim}, and CD3^{dim}CD7^{low} subpopulations in patients with acute-type ATL. We reviewed the glass-slide specimens of FACS-sorted samples to evaluate the morphology of each subpopulation on the CD3 vs CD7 plots. Representative results for two patients (no. 6 and 7) are shown in Figure 6A. In both patients, atypical lymphocytes with notched nuclei and/or basophilic cytoplasm were observed in all three subpopulations. In contrast, abnormal lymphocytes, including cells with multilobulated nuclei (flower cells) were mainly observed in the CD3^{dim}CD7^{low} subpopulation in patient no. 6 (Fig. 6, left) and in the CD3^{dim}CD7^{dim} and CD3^{dim}CD7^{low} subpopulations in patient no. 7 (Fig. 6, right panel).

Discussion

To investigate the characteristics of ATL cells, the purification of tumor cells is essential. In the present study, we successfully discriminated the CD3^{dim}CD7^{low} subpopulation in CD4$^+$ T cells in the peripheral blood of patients with acute-type ATL by constructing a CD3 vs CD7 plot of CD4$^+$ T cells from multi-color FACS (Fig. 1). Previously, Yokote et al.[10] reported that CD3^{low} gating facilitated the discrimination of ATL cells by flow cytometry. If we constructed a CD4 vs either CD3 or CD7 plot, in which the downregulated cell subpopulation was not clearly separated, then we could not define distinct cell subpopu-
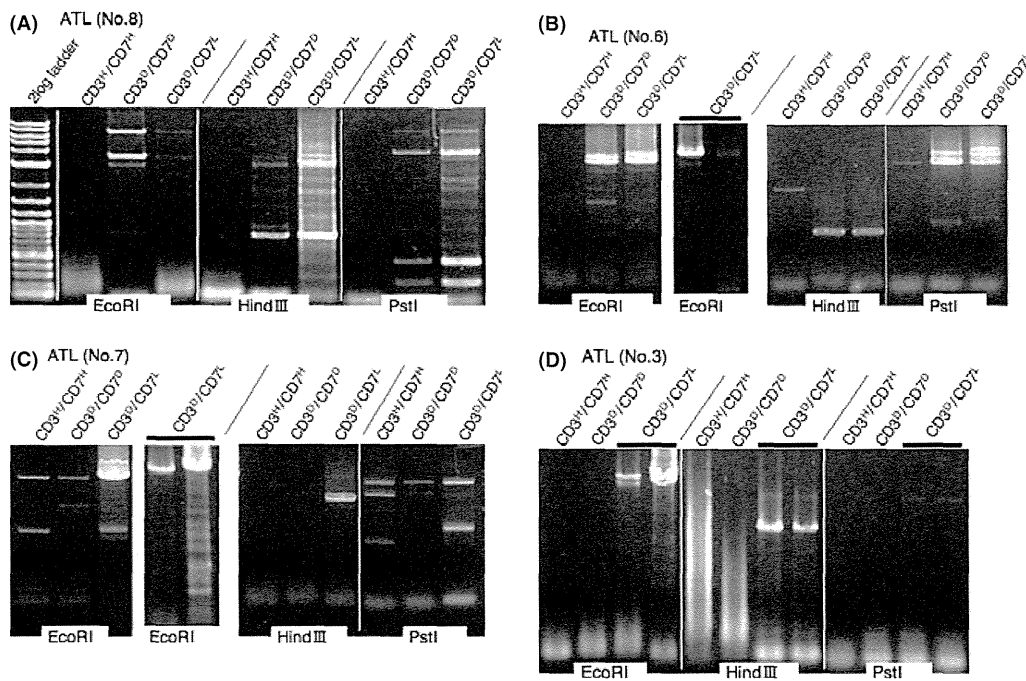

Fig. 4. Analysis of clonality in the CD3^{high}CD7^{high}, CD3^{dim}CD7^{dim} and CD3^{dim}CD7^{low} subpopulations using inverse long PCR. (A–D) Genomic DNA was extracted from FACS-sorted cells of each subpopulation and subjected to inverse long PCR. Representative data of four cases (patients no. 3, 6, 7 and 8) are shown For the CD3^{dim}CD7^{low} subpopulations of patients no. 3, 6 and 7, PCR was performed in duplicate (black bars). ATL, adult T-cell leukemia.
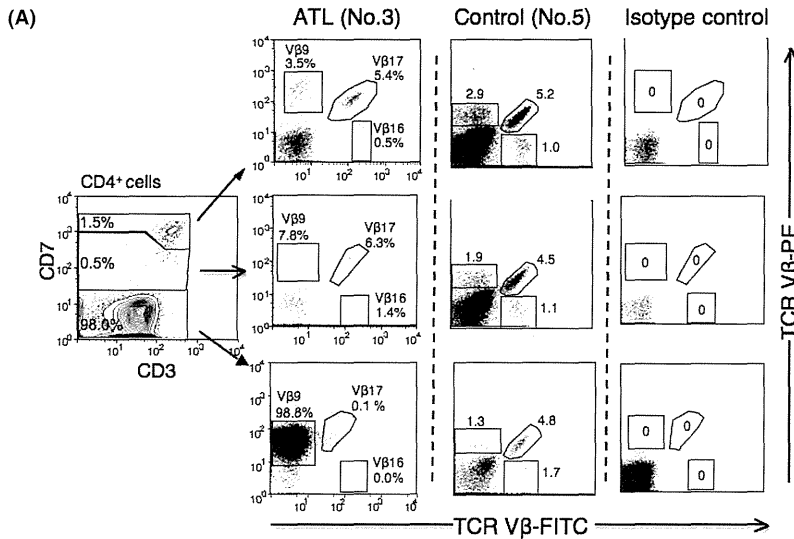
(A) ATL (No.3)   Control (No.5)   Isotype control

(B) (%)

ATL (No.3)

☐ CD3^{H}CD7^H
▨ CD3^{D}CD7^D
■ CD3^{D}CD7^L

TCR Vβ repertoire

(%)

Control (No.5)

TCR Vβ repertoire

Fig. 5. Clonality in the CD3^{high}CD7^{high}, CD3^{dim}CD7^{dim} and CD3^{dim}CD7^{low} subpopulations using flow cytometry-based T-cell receptor (TCR)-Vβ repertoire analysis. (A) Representative data are shown A monoclonal pattern of TCR-Vβ9 expression was evident in the CD3^{dim}CD7^{low} subpopulation of the adult T-cell leukemia (ATL) sample. Representative dot plots of 3 of the 24 TCR-Vβ repertoire (Vβ9, 16 and 17) are shown. (B) Bar graph representation of the data from Figure 5A. The percentages of cells positive for each TCR-Vβ repertoire in the CD3^{high}CD7^{high}, CD3^{dim}CD7^{dim} and CD3^{dim}CD7^{low} subpopulations. White bar, CD3^{high}CD7^{high}; gray bar, CD3^{dim}CD7^{dim}; black bar, CD3^{dim}CD7^{low}.

lations using the CD3 or CD7 marker alone, because the degrees of downregulation of CD3 and CD7 are variable. It should be noted that the combination of CD3 downregulation and diminished expression or absence of CD7 clearly indicates this subpopulation. In addition, gating-out monocytes in the CD4 vs CD14 plot is important for the CD3 vs CD7 plot because monocytes were CD3/CD7 dull-positive based on the nonspecific binding of the antibody.

A substantial subpopulation of T cells has been reported to be CD7-deficient under physiological[16,17] and certain pathological conditions, including autoimmune disorders and viral infection.[18–22] Consistent with these reports, the present study indicated that the proportion of CD4$^+$CD7- T cells in the peripheral blood of healthy adults is up to 10% (Fig. 1B,C). In ATL samples, the CD3 vs CD7 plot revealed various patterns, which may reflect the differences in clinical characteristics of each patient; however, the CD3^{dim}CD7^{low} subpopulation, which was a minor population in the normal controls, was prominent in all ATL samples (Fig. 1B,C). These results prompted us to study this

subpopulation in detail. Estimation of the HTLV-I proviral load by quantitative real-time PCR showed that the majority of cells in the CD3^{dim}CD7^{low} subpopulation were infected with HTLV-I (Fig. 2). Immunophenotypic analysis revealed that the expression of CD25, a common ATL marker,[9,23] and CCR4, reported to be expressed in around 90% of cases of ATL,[24,25] were upregulated in the CD3^{dim}CD7^{low} subpopulations of ATL samples in contrast to normal controls in which both markers were weakly expressed in the equivalent subpopulation (Fig. 3A,B). As several studies indicated that ATL cells originate from CD4$^+$CD25$^+$FoxP3$^+$ Treg cells,[26] we next analyzed FoxP3 expression in each subpopulation. In the CD3^{dim}CD7^{low} subpopulation, the FoxP3 expression levels were variable, consistent with previous reports.[27] In one case, FoxP3 expression was upregulated in the CD3^{high}CD7^{high} and CD3^{dim}CD7^{dim} subpopulations suggesting that they were normal Treg cells.

The analysis of clonality is extremely important for determining whether cells are transformed and Southern blot analysis is usually used to confirm clonality. However, in the present study,
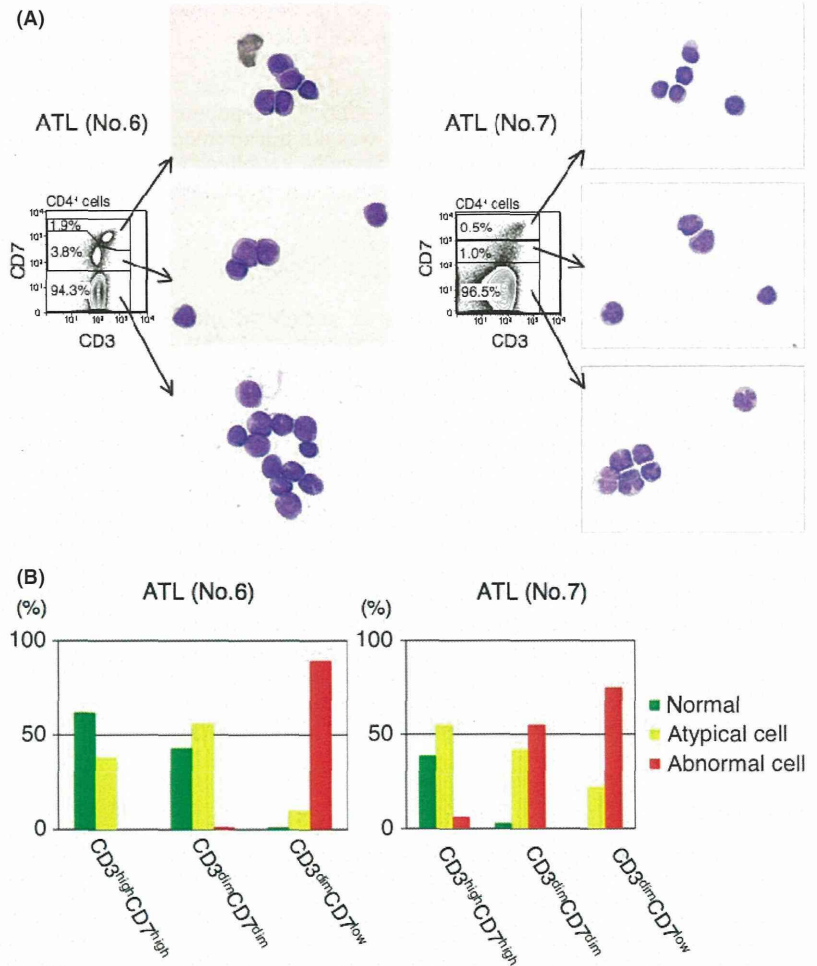
(A)

ATL (No.6)

ATL (No.7)

CD4⁺ cells

CD7 / CD3

1.9%
3.8%
94.3%

CD4⁺ cells

CD7 / CD3

0.5%
1.0%
96.5%

(B)

Fig. 6. Morphology of the CD3^{high}CD7^{high}, CD3^{dim}CD7^{dim} and CD3^{dim}CD7^{low} subpopulations in two representative adult T-cell leukemia (ATL) samples (patients no. 6 and 7). (A) May–Giemsa staining of FACS-sorted cells from each subpopulation from two patients with acute-type ATL. Top, CD3^{high}CD7^{high} subpopulation; middle, CD3^{dim}CD7^{dim} subpopulation; bottom, CD3^{dim}CD7^{low} subpopulation. (B) Percentages of cells with different morphology in each subpopulation. Normal, lymphocytes with normal morphology; atypical, lymphocytes with notched nuclei and basophilic cytoplasm; abnormal, lymphocytes with convoluted, deeply indented or multilobulated flower cells.

the cell number following cell sorting was not sufficient for Southern blotting, and thus inverse long PCR for clonality analysis of HTLV-I-infected cells was used.[25] Studies of four ATL samples revealed clonal expansion of ATL cells in the CD3^{dim}CD7^{low} subpopulations, although minor clones may exist in the population (Fig. 4). When PCR was performed in duplicate, we found that the major bands were consistently detected in all cases. However, the detection of multiple minor bands was not consistent. As reported previously, the inverse long PCR method stochastically amplifies the template originating from small clones.[28,29] The minor bands observed in the present study will contain small clones. However, the presence of nonspecific bands cannot be eliminated.

The inverse long PCR method is commonly used for clonality analysis; however, it cannot quantify the size of major/minor clones and the degree of enrichment in each subpopulation. Therefore, we tested the FACS-based TCR-Vβ repertoire analysis combined with our multi-color FACS system (Fig. 5). In ATL patient no. 3, almost all cells in the CD3^{dim}CD7^{low} subpopulations were clonal cells with TCR-Vβ9. Inverse long PCR analysis in the same patient showed multiple minor bands in the CD3^{dim}CD7^{low} subpopulations (Fig. 4D). These results did not conflict with those of the TCR-Vβ repertoire analysis, as the inverse long PCR method is a more sensitive method for detecting small clones compared with flow cytometry. Taken together, the series of analyses in the present study indicated that the CD3^{dim}CD7^{low} subpopulations consist of highly purified ATL cells in patients with acute-type ATL.

A substantial proportion of cells in the CD3^{dim}CD7^{dim} subpopulation consisted of morphologically abnormal lymphocytes (Fig. 6) that exhibited upregulation of CD25 and CCR4 expression (Fig. 3A,B). Using the inverse long PCR method, a similar band pattern between CD3^{dim}CD7^{dim} and CD3^{dim}CD7^{low} subpopulations was observed in patients no. 6 and 8, suggesting that these cells belonged to the same clone (Fig. 4A,B). However, not all of the cells in this subpopulation were infected with HTLV-I because the HTLV-I proviral load was less than that of the CD3^{dim}CD7^{low} subpopulation (Fig. 2). Thus, at least a small number of the CD3^{dim}CD7^{dim} cells were expected to be ATL cells. Those cells observed in the CD3^{dim}CD7^{dim} subpopulation that were phenotypically different from the CD3^{dim}CD7^{low} subpopulations were of particular interest. We detected a band of the same size on inverse long PCR in the CD3^{dim}CD7^{dim} subpopulations as in the CD3^{dim}CD7^{low} subpopulation. This may have been because the two subpopulations originated from the same clone that evolved from a CD3^{dim}CD7^{dim} to a CD3^{dim}CD7^{low} phenotype. Further studies are required to determine the characteristics of the CD3^{dim}CD7^{dim} subpopulation in greater detail.

The results of the present study indicated that HTLV-I-infected cells distribute from a CD7^{high} to a CD7^{low} subpopulation, although the proportion of HTLV-I-infected cells was remarkably low in the CD3^{high}CD7^{high} subpopulation (Fig. 2). A considerable proportion of cells in the CD3^{high}CD7^{high} subpopulation consisted of morphologically atypical lymphocytes (Fig. 6), but the CD25 and CCR4 levels were not upregulated

(Fig. 3A,B). When analyzing the pattern of the inverse long PCR of the CD3^{high}CD7^{high} subpopulations, we observed a difference from those of the CD3^{dim}CD7^{dim} and CD3^{dim}CD7^{low} subpopulations (Fig. 4). In patients no. 6 (Fig. 4B) and 7 (Fig. 4C), the band detected in the CD3^{high}CD7^{high} subpopulation may represent an expanded clone that was not transformed. Most likely, these cells do not represent ATL cells, but oligoclonal HTLV-I-infected lymphocytes. Previous studies indicated that HTLV-I-infected cells undergo transformation through multi-step oncogenesis.[30] A detailed analysis of these three subpopulations may therefore provide some insight into the oncogenesis of HTLV-I-infected cells.

Accurate determination of ATL cells in peripheral blood is critical for estimating the response to chemotherapy. However, as discussed above, morphological studies (Fig. 6) have limitations in their ability to discriminate ATL from non-ATL cells.[31,32]. Recently, hematopoietic stem cell transplantation has been explored as a promising treatment to overcome the poor prognosis of this most incurable lymphoid malignancy,[33,34] and monitoring minimal residual disease following hematopoietic stem cell transplantation is more important. Our method of analyzing ATL cells may be particularly useful for monitoring minimal residual disease. Although the CD3^{dim}CD7^{dim} subpopulation in our analysis may have included some ATL cells, this is a minor population in the peripheral blood of patients with acute-type ATL, and it is sufficient for practical use to monitor the CD3^{dim}CD7^{low} subpopulation. Another possible use of our procedure is for the definitive classification of ATL subtypes according to Shimoyama's criteria.[8] A proportion of abnormal lymphocytes in peripheral blood comprise part of the criteria for ATL-subtype classification but it is sometimes confusing. Our multi-color FACS system may clearly quantify this proportion.

In conclusion, we have constructed a multi-color FACS system to purify ATL cells in the peripheral blood of patients with acute-type ATL. This system may be useful for precisely monitoring the disease during chemotherapy, detecting minimal residual disease and analyzing ATL cells. This system may be of great benefit in investigating oncogenesis in HTLV-I-infected cells.

Acknowledgments

Disclosure Statement

The authors declare no financial conflicts of interest.

References

1 Yoshida M, Miyoshi I, Hinuma Y. Isolation and characterization of retrovirus from cell lines of human adult T-cell leukemia and its implication in the disease. Proc Natl Acad Sci U S A 1982; 79 (6): 2031–5.

2 Matsuoka M. Human T-cell leukemia virus type I (HTLV-I) infection and the onset of adult T-cell leukemia (ATL). Retrovirology 2005; 2: 27.

3 Nicot C. Current views in HTLV-I-associated adult T-cell leukemia/lymphoma. Am J Hematol 2005; 78 (3): 232–9.

4 Ginaldi L, Matutes E, Farahat N, De Martinis M, Morilla R, Catovsky D. Differential expression of CD3 and CD7 in T-cell malignancies: a quantitative study by flow cytometry. Br J Haematol 1996; 93 (4): 921–7.

5 Campana D, Coustan-Smith E. Minimal residual disease studies by flow cytometry in acute leukemia. Acta Haematol 2004; 112 (1–2): 8–15.

6 Craig FE, Foon KA. Flow cytometric immunophenotyping for hematologic neoplasms. Blood 2008; 111 (8): 3941–67.

7 Akl H, Badran B, Dobirta G et al. Progressive loss of CD3 expression after HTLV-I infection results from chromatin remodeling affecting all the CD3 genes and persists despite early viral genes silencing. Virol J 2007; 4: 85.

8 Shimoyama M. Diagnostic criteria and classification of clinical subtypes of adult T-cell leukaemia-lymphoma. A report from the Lymphoma Study Group (1984–87). Br J Haematol 1991; 79 (3): 428–37.

9 Tsukasaki K, Hermine O, Bazarbachi A et al. Definition, prognostic factors, treatment, and response criteria of adult T-cell leukemia-lymphoma: a proposal from an international consensus meeting. J Clin Oncol 2009; 27 (3): 453–9.

10 Yokote T, Akioka T, Oka S et al. Flow cytometric immunophenotyping of adult T-cell leukemia/lymphoma using CD3 gating. Am J Clin Pathol 2005; 124 (2): 199–204.

11 Yamada Y, Tomonaga M, Fukuda H et al. A new G-CSF-supported combination chemotherapy, LSG15, for adult T-cell leukaemia-lymphoma: Japan Clinical Oncology Group Study 9303. Br J Haematol 2001; 113 (2): 375–82.

12 Roncador G, Brown PJ, Maestre L et al. Analysis of FOXP3 protein expression in human CD4+CD25+ regulatory T cells at the single-cell level. Eur J Immunol 2005; 35 (6): 1681–91.

13 Iwanaga M, Watanabe T, Utsunomiya A et al. Human T-cell leukemia virus type I (HTLV-I) proviral load and disease progression in asymptomatic HTLV-I carriers: a nationwide prospective study in Japan. Blood 2010; 116 (8): 1211–19.

14 Sakaguchi S. Naturally arising Foxp3-expressing CD25+CD4+ regulatory T cells in immunological tolerance to self and non-self. Nat Immunol. 2005; 6 (4): 345–52.

15 Morice WG, Kimlinger T, Katzmann JA et al. Flow cytometric assessment of TCR-Vbeta expression in the evaluation of peripheral blood involvement by T-cell lymphoproliferative disorders: a comparison with conventional T-cell immunophenotyping and molecular genetic techniques. Am J Clin Pathol 2004; 121 (3): 373–83.

16 Reinhold U, Abken H. CD4+ CD7- T cells: a separate subpopulation of memory T cells? J Clin Immunol 1997; 17 (4): 265–71.

17 Reinhold U, Abken H, Kukel S et al. CD7- T cells represent a subset of normal human blood lymphocytes. J Immunol 1993; 150 (5): 2081–9.

18 Aandahl EM, Quigley MF, Moretto WJ et al. Expansion of CD7(low) and CD7(negative) CD8 T-cell effector subsets in HIV-1 infection: correlation with antigenic load and reversion by antiretroviral treatment. Blood 2004; 104 (12): 3672–8.

19 Autran B, Legac E, Blanc C, Debre P. A Th0/Th2-like function of CD4 + CD7- T helper cells from normal donors and HIV-infected patients. J Immunol 1995; 154 (3): 1408–17.

20 Legac E, Autran B, Merle-Beral H, Katlama C, Debre P. CD4+CD7-CD57+ T cells: a new T-lymphocyte subset expanded during human immunodeficiency virus infection. Blood 1992; 79 (7): 1746–53.

21 Schmidt D, Goronzy JJ, Weyand CM. CD4+ CD7- CD28- T cells are expanded in rheumatoid arthritis and are characterized by autoreactivity. J Clin Invest 1996; 97 (9): 2027–37.

22 Willard-Gallo KE, Van de Keere F, Kettmann R. A specific defect in CD3 gamma-chain gene transcription results in loss of T-cell receptor/CD3 expression late after human immunodeficiency virus infection of a CD4+ T-cell line. Proc Natl Acad Sci U S A 1990; 87 (17): 6713–17.

23 Matsuoka M, Jeang KT. Human T-cell leukaemia virus type 1 (HTLV-I) infectivity and cellular transformation. Nat Rev Cancer 2007; 7 (4): 270–80.

24 Ishida T, Utsunomiya A, Iida S et al. Clinical significance of CCR4 expression in adult T-cell leukemia/lymphoma: its close association with skin involvement and unfavorable outcome. Clin Cancer Res 2003; 9 (10 Pt 1): 3625–34.

25 Yoshie O, Fujisawa R, Nakayama T et al. Frequent expression of CCR4 in adult T-cell leukemia and human T-cell leukemia virus type 1-transformed T cells. Blood 2002; 99 (5): 1505–11.

26 Yano H, Ishida T, Inagaki A et al. Regulatory T-cell function of adult T-cell leukemia/lymphoma cells. Int J Cancer 2007; 120 (9): 2052–7.

27 Abe M, Uchihashi K, Kazuto S et al. Foxp3 expression on normal and leukemic CD4+CD25+ T cells implicated in human T-cell leukemia virus type-1 is inconsistent with Treg cells. Eur J Haematol 2008; 81 (3): 209–17.

28 Tanaka G, Okayama A, Watanabe T *et al.* The clonal expansion of human T lymphotropic virus type 1-infected T cells: a comparison between seroconverters and long-term carriers. *J Infect Dis* 2005; **191** (7): 1140–7.

29 Cavrois M, Wain-Hobson S, Wattel E. Stochastic events in the amplification of HTLV-I integration sites by linker-mediated PCR. *Res Virol* 1995; **146** (3): 179–84.

30 Verdonck K, Gonzalez E, Van Dooren S, Vandamme AM, Vanham G, Gotuzzo E. Human T-lymphotropic virus 1: recent knowledge about an ancient infection. *Lancet Infect Dis* 2007; **7** (4): 266–81.

31 Sakamoto Y, Kawachi Y, Uchida T *et al.* Adult T-cell leukaemia/lymphoma featuring a large granular lymphocyte leukaemia morphologically. *Br J Haematol* 1994; **86** (2): 383–5.

32 Tsukasaki K, Imaizumi Y, Tawara M *et al.* Diversity of leukaemic cell morphology in ATL correlates with prognostic factors, aberrant immunophenotype and defective HTLV-I genotype. *Br J Haematol* 1999; **105** (2): 369–75.

33 Okamura J, Utsunomiya A, Tanosaki R *et al.* Allogeneic stem-cell transplantation with reduced conditioning intensity as a novel immunotherapy and antiviral therapy for adult T-cell leukemia/lymphoma. *Blood* 2005; **105** (10): 4143–5.

34 Utsunomiya A, Miyazaki Y, Takatsuka Y *et al.* Improved outcome of adult T-cell leukemia/lymphoma with allogeneic hematopoietic stem cell transplantation. *Bone Marrow Transplant.* 2001; **27** (1): 15–20.

CpG island methylation of microRNAs is associated with tumor size and recurrence of non-small-cell lung cancer

Kentaro Kitano,[1,6] Kousuke Watanabe,[2,6] Noriko Emoto,[2] Hidenori Kage,[2] Emi Hamano,[2] Takahide Nagase,[2] Atsushi Sano,[1] Tomohiro Murakawa,[1] Jun Nakajima,[1] Akiteru Goto,[3] Masashi Fukayama,[3] Yutaka Yatomi,[4] Nobuya Ohishi[2] and Daiya Takai[4,5]

[1]Department of Thoracic Surgery, [2]Department of Respiratory Medicine, [3]Department of Pathology, [4]Department of Clinical Laboratory, The University of Tokyo Hospital, Tokyo, Japan

We investigated whether the CpG island methylation of certain microRNAs was associated with the clinicopathological features and the prognosis of non-small-cell lung cancer. The methylation of mir-152, -9-3, -124-1, -124-2, and -124-3 was analyzed in 96 non-small-cell lung cancer specimens using a combined bisulfite restriction analysis. The median observation period was 49.5 months. The methylation of mir-9-3, -124-2, and -124-3 was individually associated with an advanced T factor independent of age, sex, and smoking habit. Moreover, the methylation of multiple microRNA loci was associated with a poorer progression-free survival in a univariate analysis. Our result enlightens the accumulation of aberrant DNA methylation which occurs in concordance with the tumor progression. (Cancer Sci 2011; 102: 2126–2131)

L ung cancer is the leading cause of cancer-related mortality in the world,[1] and non-small-cell lung cancer (NSCLC) is the most common type. Surgical resection remains the only curative treatment for NSCLC. Identifying factors that are associated with aggressive disease may lead to the development of novel biomarkers and the identification of therapeutic targets that can help reduce the burden of this disease.

MicroRNAs (miRNAs) are a class of small non-coding RNAs that negatively regulate target gene expression by accelerating the degradation of mRNA and translational inhibition, with potentially hundreds of target mRNAs.[2] They influence a variety of cellular functions including proliferation, differentiation, and apoptosis.[3] Specific miRNAs can behave as either tumor suppressor genes or oncogenes, depending on the tissue type and the presence of specific targets.[4,5]

More than 100 species of known miRNAs are embedded within or near the CpG islands of the human genome and are potentially subject to control by epigenetic alterations such as DNA methylation and histone modification. Systematic assessments of miRNA expression and epigenetic modifications among cell lines and primary tumor specimens have revealed the existence of the epigenetic regulation of miRNAs in multiple tumor types.[6–9]

The goals of this study were to explore possible relationships between the methylation profiles of miRNAs and the clinicopathological characteristics of NSCLC patients and to identify new specific methylation markers capable of detecting advanced pathological features.

In the present study, the methylation status of five miRNA loci within five separate CpG islands was determined in 96 NSCLC tissue specimens. The choice of the miRNAs was based on our previous study[9] as well as other published reports.[10,11] Our data show that the CpG island methylation of miRNAs is common in NSCLC, and that the methylation of multiple miRNA loci is associated with an advanced T status as well as the progression-free survival (PFS) of patients with NSCLC.

Materials and Methods

Patients. We collected cancer tissues and normal lung tissues from NSCLC patients who underwent surgical resection at the University of Tokyo Hospital (Tokyo, Japan) between June 2005 and September 2007 after receiving approval from the Institutional Ethics Review Committee and after obtaining informed consent from all patients. The diagnoses were based on pathological evidence and were classified according to the TNM classification criteria.[12] To circumvent statistical disruption arising from the heterogeneity of significantly advanced diseases, patients whose tumors were pathologically confirmed as T3 or T4 were excluded.

Combined bisulfite restriction analysis (COBRA). DNA was extracted by the standard proteinase K and phenol method.[13] One microgram of genomic DNA was bisulfite treated and purified, according to the protocol described previously.[14,15] The bisulfite-treated DNA was amplified by PCR using AmpliTaq Gold 360 Master Mix (Applied Biosystems, Foster City, CA, USA). The PCR product was treated with ExoSAP-IT (US Biochemical, Cleveland, OH, USA) to improve the visibility of the band.[16] The product was digested with the restriction enzymes BstUI or BssHII (New England Biolabs, Ipswich, MA, USA). To dissociate the tightly bound enzymes from the DNA, the digested product was purified using phenol–chloroform extraction when necessary. The DNA was visualized by 2% agarose gel electrophoresis with the addition of a loading buffer containing SDS (final concentration, 0.1%) and was identified as methylation-positive if an appropriately sized band was present.

Statistics. A statistical analysis was carried out using JMP 7 software (SAS Institute, Cary, NC, USA). The difference in frequencies was assessed using a χ^2-test. The risks of advanced pathological features were analyzed using a multivariate logistic regression analysis. Progression-free survival curves were calculated using the Kaplan–Meier method and compared using a log–rank test. A P-value of <0.05 was considered significant.

Results

Characteristics of the patients. A total of 96 cases were analyzed. The baseline characteristics of the patient cohort are shown in Table 1. The median follow-up period was

[5]To whom correspondence should be addressed. E-mail: dtakai-ind@umin.ac.jp
[6]These authors contributed equally to this work.

Table 1. Baseline characteristics of 96 patients with non-small-cell lung carcinoma

Characteristics	Patient cohort (n = 96)
Age, years	
Median	66
Interquartile range	59–72
Sex, n (%)	
Male	60 (62.5)
Female	36 (37.5)
Smoking habit, n (%)	
Never	33 (34.4)
Ever	63 (65.6)
Histological type, n (%)	
Adenocarcinoma	78 (81.3)
Squamous cell carcinoma	17 (17.7)
Adenosquamous carcinoma	1 (1.0)
Stage, n (%)	
IA	41 (42.7)
IB	26 (27.1)
IIA	5 (5.2)
IIB	7 (7.3)
IIIA	17 (17.7)
T factor, n (%)	
T1	54 (56.3)
T2	42 (43.8)
N factor, n (%)	
N0	67 (69.8)
N1	12 (12.5)
N2	17 (17.7)
Lymphatic invasion, n (%)	
Negative	72 (75.0)
Positive	24 (25.0)
Vascular invasion, n (%)	
Negative	58 (60.4)
Positive	38 (39.6)
EGFR mutation, n (%)	
Negative	65 (67.7)
Positive	27 (28.1)
Unknown	4 (4.2)

EGFR, epidermal growth factor receptor; n, number of cases.
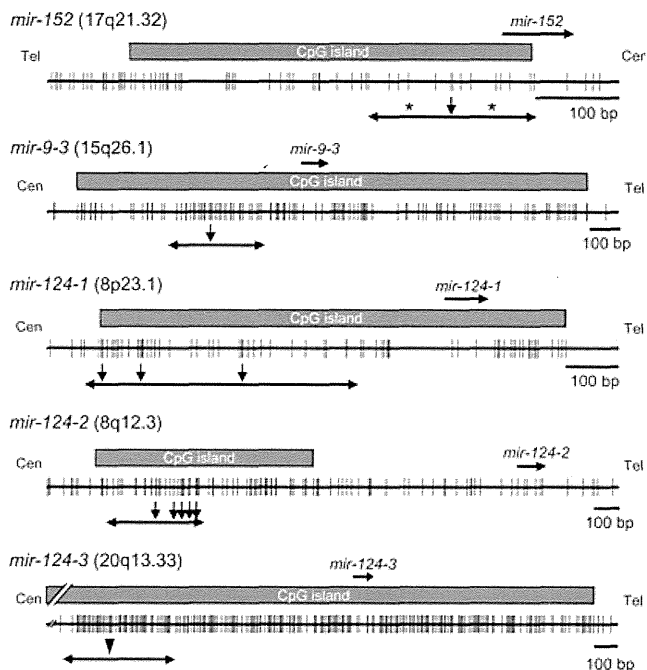

Fig. 1. Gene maps around the CpG islands in relation to *mir-152*, *-9-1*, *-9-3*, *-124-1*, *-124-2*, and *-124-3*. For combined bisulfite restriction analysis, PCR products were restricted using *Bst*UI (vertical downward arrows) or *Bss*HII (closed arrowheads). Gray boxes, CpG islands; horizontal bidirectional arrows, PCR products; stars, both fragments were designed to be equal in size to emphasize the visualization of the restricted PCR products; vertical tick marks, CpG sites.

49.5 months. A total of 30 patients developed recurrent disease during the observation period. The most frequent recurrent site was the brain (46.7%), followed by the lymph nodes (23.3%), bone (13.3%), and the lungs (10.0%).

miRNA loci analyzed in COBRA. We focused on *miR-152*, the methylation of which has never been documented in lung can-

cer. In addition, we included *miR-9* and *miR-124*, the methylation of which has been previously reported in lung cancer.[10,11] In the human genome, *miR-9* and *miR-124* are each located at three distinct loci: *mir-9-1*, *-9-2*, *-9-3*; and *mir-124-1*, *-124-2*, and *-124-3*. *MiR-152* is located at a single locus: *mir-152*. All of these loci are embedded within CpG islands, except for *mir-9-2*. We first carried out COBRA using tumor and adjacent normal tissues from eight NSCLC cases (Fig. S1). The locus *mir-9-1* was excluded from the study because no tumor-specific methylation was observed. The gene maps, primer sequences, annealing temperatures, and restriction enzymes used for COBRA are shown in Figure 1 and Table 2.

Relationships between CpG island methylation of the miRNAs and the clinicopathological features of 96 NSCLC patients. The methylation profiles of the five miRNA loci were obtained

Table 2. Primer sequences, PCR characteristics, and restriction enzymes for combined bisulfite restriction analysis

miRNA	Locus		Primers from 5′ to 3′	Product size (bp)	Ta (°C)	Restriction enzyme
mir-152	17q21.32	Forward	GGGGAGGGTAAGGAGTGGTTTGT	202	55	*Bst*UI†
		Reverse	CCRAATCRAAATATATCACAAAACCTA‡			
mir-9-3	15q26.1	Forward	TTTGAATGGGAGTTTGTGATTGG	327	55	*Bst*UI
		Reverse	AAAAACCATATAAAAAACTAAAATATATAA			
mir-124-1	8p23.1	Forward	AGGTTGAATTTTTAGGTTTTAGTTT	521	55	*Bst*UI
		Reverse	AAAAACCACAACATCCTCC			
mir-124-2	8q12.3	Forward	GTTTTGTAGTTTGTAGGGTTTTAAA	378	55	*Bst*UI
		Reverse	CAAAAAAACAAAACCCCAAT			
mir-124-3	20q13.33	Forward	AGAAGGGAGTTAGGTAAGTTTT	474	50	*Bss*HII
		Reverse	AAAAACCATATAAAAAACTAAAATATATAA			

†Phenol–chloroform extraction was needed after the digestion for clear vision of bands. ‡Two kinds of reverse primers, which changed a part of R into G or A, were mixed and used to amplify the bisulfite-modified genomic DNA. Ta, annealing temperature.